Sodium-Ion Batteries

Deutsche Ausgabe: DOI: 10.1002/ange.201607469
Internationale Ausgabe: DOI: 10.1002/anie.201607469

Cobalt-Doped FeS_2 Nanospheres with Complete Solid Solubility as a High-Performance Anode Material for Sodium-Ion Batteries

Kai Zhang, Mihui Park, Limin Zhou, Gi-Hyeok Lee, Jeongyim Shin, Zhe Hu, Shu-Lei Chou, Jun Chen, and Yong-Mook Kang**

Abstract: *Considering that the high capacity, long-term cycle life, and high-rate capability of anode materials for sodium-ion batteries (SIBs) is a bottleneck currently, a series of Co-doped FeS_2 solid solutions with different Co contents were prepared by a facile solvothermal method, and for the first time their Na-storage properties were investigated. The optimized $Co_{0.5}Fe_{0.5}S_2$ (Fe0.5) has discharge capacities of 0.220 Ah g^{-1} after 5000 cycles at 2 A g^{-1} and 0.172 Ah g^{-1} even at 20 A g^{-1} with compatible ether-based electrolyte in a voltage window of 0.8–2.9 V. The Fe0.5 sample transforms to layered $Na_xCo_{0.5}Fe_{0.5}S_2$ by initial activation, and the layered structure is maintained during following cycles. The redox reactions of $Na_xCo_{0.5}Fe_{0.5}S_2$ are dominated by pseudocapacitive behavior, leading to fast Na^+ insertion/extraction and durable cycle life. A $Na_3V_2(PO_4)_3$/Fe0.5 full cell was assembled, delivering an initial capacity of 0.340 Ah g^{-1}.*

Sodium-ion batteries (SIBs) are highly attractive as a promising battery system in a post Li-ion battery (LIB) era because sodium precursors are cheap and abundant.[1] To date, learning from LIBs, high-capacity anode materials for SIBs include simple substances, alloys, and transition-metal chalcogenides.[2–4] Among them, transition-metal disulfides (TMDSs) have received remarkable interests owing to their robust structure, low cost, simple preparation, and high theoretical capacities.[3–7] To further improve their electrochemical properties, many reports have focused on introducing conductive carbon materials to enhance electronic conductivity and accommodate volume changes during charge–discharge process.[8] However, the carbon contents are typically more than 40 wt%, which reduces a practical capacity of the electrode. Furthermore, it is still difficult to retain a high capacity after over 1000 cycles or at a high current rate of above 10 A g^{-1}. Thus, it is urgent and necessary to propose novel solutions to develop high-capacity TMDSs with stable cyclic retention and high rate capability.

To address these problems, controlling discharge cut-off voltages and utilizing an ether-based electrolyte (1M $NaSO_3CF_3$ in diglyme (DGM)) have been attempted for TMDSs without the carbon modification.[5,9] Raising the discharge cut-off voltage prohibits conversion reactions and makes intercalation reactions take place during charge–discharge cycles. The ether-based electrolytes present a higher chemical stability with intermediate products of TMDSs during charge/discharge than the carbonate-based electrolytes. Nevertheless, a single TMDS is difficult to meet all the requirements as a promising electrode material. Thus, in term of intrinsic feature of substance, it would be interesting to know if binary TMDSs could integrate their own advantages.

FeS_2, as an easily accessible natural mineral, shows good cycling and rate performance when cycling between 0.8–2.9 V.[9] However, its capacity needs be further enhanced. Fu's group first reported Na-storage property of CoS_2 with an ether-based electrolyte.[6] The CoS_2 delivered a higher capacity in a voltage range of 1.0–2.9 V than that of FeS_2, but its rate performance is worse than that of FeS_2. Because CoS_2 has similar pyrite structure to FeS_2, Co^{2+} ions can be doped into FeS_2 to form a complete solid solution,[10] inspiring us to prepare Co-doped FeS_2 to combine the high rate capability of FeS_2 and high capacity of CoS_2.

Herein, a series of Co-doped FeS_2 with different Co contents have been synthesized by a facile one-step solvothermal route and for the first time used as anode materials for SIBs. $Co_{0.5}Fe_{0.5}S_2$ sample exhibits the best electrochemical performance among the doping series, FeS_2, and CoS_2. It delivers a discharge capacity of 0.220 Ah g^{-1} after 5000 cycles at 2 A g^{-1}. Even at 20 A g^{-1}, discharge capacity is still 0.172 Ah g^{-1}. Moreover, $Na_3V_2(PO_4)_3$/$Co_{0.5}Fe_{0.5}S_2$ full cell shows an initial capacity of 0.340 Ah g^{-1}.

The Co-doped FeS_2 was synthesized by a simple solvothermal route (see the Experimental Section in the Supporting Information). According to the concentration ratio of $FeSO_4{\cdot}7H_2O$ to $CoSO_4{\cdot}7H_2O$ (x: $(1-x)$ ($x = 1.0$, 0.9, 0.7, 0.5, 0.4, and 0.0)), the corresponding samples are referred to as FeS_2, Fe0.9, Fe0.7, Fe0.5, Fe0.4, and Fe0.0, respectively. Figure 1 a and the Supporting Information, Figure S1 show X-ray diffraction (XRD) patterns of the as-prepared six samples. When x is more than or equal to 0.5, all diffraction peaks can be indexed to the standard JCPDS No. 71-53, indicating that they have a cubic pyrite phase with the $Pa\bar{3}$ space group. CoS_2

[*] Dr. K. Zhang, M. Park, G.-H. Lee, J. Shin, Prof. Y.-M. Kang
Department of Energy and Materials Engineering
Dongguk University-Seoul
Seoul 04620 (Republic of Korea)
E-mail: dake1234@dongguk.edu
L. Zhou, Prof. J. Chen
Key Laboratory of Advanced Energy Materials Chemistry (Ministry of Education), Collaborative Innovation Center of Chemical Science and Engineering, College of Chemistry, Nankai University
Tianjin 300071 (China)
E-mail: chenabc@nankai.edu.cn
Dr. Z. Hu, Dr. S.-L. Chou
Institute for Superconducting and Electronic Materials
University of Wollongong
Wollongong, New South Wales 2522 (Australia)

Supporting information for this article can be found under: http://dx.doi.org/10.1002/anie.201607469.

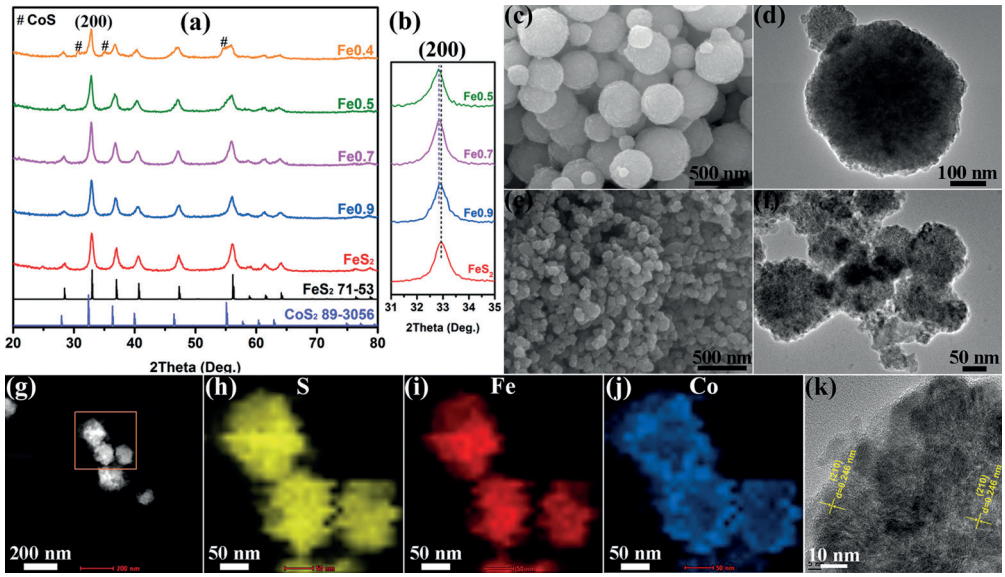

Figure 1. a) XRD patterns of the as-prepared FeS_2, Fe0.9, Fe0.7, Fe0.5, and Fe0.4 samples and b) the corresponding partial magnification patterns in a 2θ range of 31–35°. c), e) SEM and d), f) TEM images of the as-prepared FeS_2 (c, d) and Fe0.5 (e, f) samples. g)–j) EDS color mapping images and k) high-resolution TEM (HRTEM) of the Fe0.5 sample.

and any other impurities are not observed in the four doping samples. The partial magnification of the (200) peaks are displayed in Figure 1 b. After the Co doping, the (200) peaks of the Fe0.9, Fe0.7, and Fe0.5 powders shift slightly to lower angles. When $x = 0.4$, CoS phase is detected at 30.6°, 35.2°, and 54.6°, suggesting that the Fe0.4 sample is impure. Besides, the results of energy dispersive spectrometer (EDS) and inductively coupled plasma-atomic emission spectroscopy (ICP-AES) demonstrate that the compositions of the Fe0.9, Fe0.7, and Fe0.5 powders are $Co_{0.1}Fe_{0.9}S_2$, $Co_{0.3}Fe_{0.7}S_2$, and $Co_{0.5}Fe_{0.5}S_2$, respectively (Supporting Information, Figure S2 and Table S1). All peaks of the as-prepared Fe0.0 sample are matched to the standard JCPDS No. 65-8977 (Supporting Information, Figure S1). It illustrates that the product is CoS when raw materials do not include Fe salts in the given synthetic condition. The composition of the Fe0.9, Fe0.7, Fe0.5, Fe0.4, and Fe0.0 samples is summarized in the Supporting Information, Table S2. The first three samples are pyrite phase, the Fe0.4 powder includes both pyrite phase and impure CoS, and the Fe0.0 sample is CoS.

Figure 1 c–f and the Supporting Information, Figure S3 display scanning electron microscopy (SEM) and transmission electron microscopy (TEM) images of the as-prepared FeS_2 and Fe0.5 powders. All samples show spherical particle shapes, but FeS_2 and the Co-doped FeS_2 samples have notably different sizes. The average diameter of FeS_2 particles is about 500 nm, while the Fe0.9, Fe0.7, and Fe0.5 particles exhibit similar average diameters of about 100 nm. Furthermore, the particle surface is slightly damaged after the Co doping. The selected area electron diffraction (SAED) patterns of the four samples in the Supporting Information, Figure S4 show that lattice spacing of the (200) plane slightly increases after the Co doping, which is in accordance with the XRD patterns in Figure 1 b. Energy-dispersive X-ray spectroscopy (EDS) mapping images of the Fe0.5 sample clearly indicate that Co shows a distinct contrast at the edge of the particles while Fe signal blurs at the edges (Figure 1 g–j). In the bulk, S, Fe, and Co are distributed uniformly. EDS line scan data (Supporting Information, Figure S5) confirms that Co concentration is much higher than Fe content at the edge of the particles. The formation process of the Co-doped FeS_2 is shown in the Supporting Information, Figure S6. Because Co^{2+} and S^{2-} ions tend to form hexagonal CoS rather than CoS_2 when raw materials do not include Fe salts under the given synthesis conditions, Co-doped FeS_2 samples originate from the ionic exchange between the initial FeS_2 nuclei and Co^{2+} ions. As a result, the diameter of the Co-doped FeS_2 is smaller than that of FeS_2, and the nanospheres has slightly damaged edge and high Co content on the edge (Supporting Information, page 8). The HRTEM image of the Fe0.5 sample (Figure 1 k) reveals that lattices in the surface and the center of the particles have the same spacing, indicating that the Fe0.5 sample is a complete solid solution despite the concentration gradient.

Figure 2 presents electrochemical properties of the as-prepared FeS_2, Fe0.9, Fe0.7, Fe0.5, and Fe0.4 powders. Before the test, the liquid electrolyte and operating voltage range were optimized first. Only charging/discharging between 0.8 and 2.9 V with ether-based electrolytes shows good cycle life. Upgrading the discharge terminal voltage avoids the conversion reactions to enable structural stability (Supporting Information, Figures S7, S8). Ether-based electrolytes show not only chemical stability with polysulfides but also solvent-co-intercalation behaviors (Supporting Information, Figure S9–S12). Figure 2 a compares their cycling performance. As Co content increases, the first discharge capacities increase. However, after 400 cycles, the Fe0.5 sample shows the highest capacity, and the Fe0.4 sample displays the lowest capacity. The cycling performance of the Fe0.0 (CoS) sample with a discharge capacity of only 0.065 Ah g^{-1} after 150 cycles is depicted in the Supporting Information, Figure S13. Since the Fe0.4 sample consists of the Co-doped FeS_2 and impure CoS, the capacity decreases more sharply than those of the other samples. Figure 2 b shows typical charge–discharge voltage curves of the five samples. FeS_2 and all of the Co-doped FeS_2 solid solution displayed three discharge voltage plateaus at about 1.7, 1.5, and 1.1 V as well as one charge slope combined with multi-step reactions. The average voltage for charge–discharge process is around 1.5 V, which is similar to

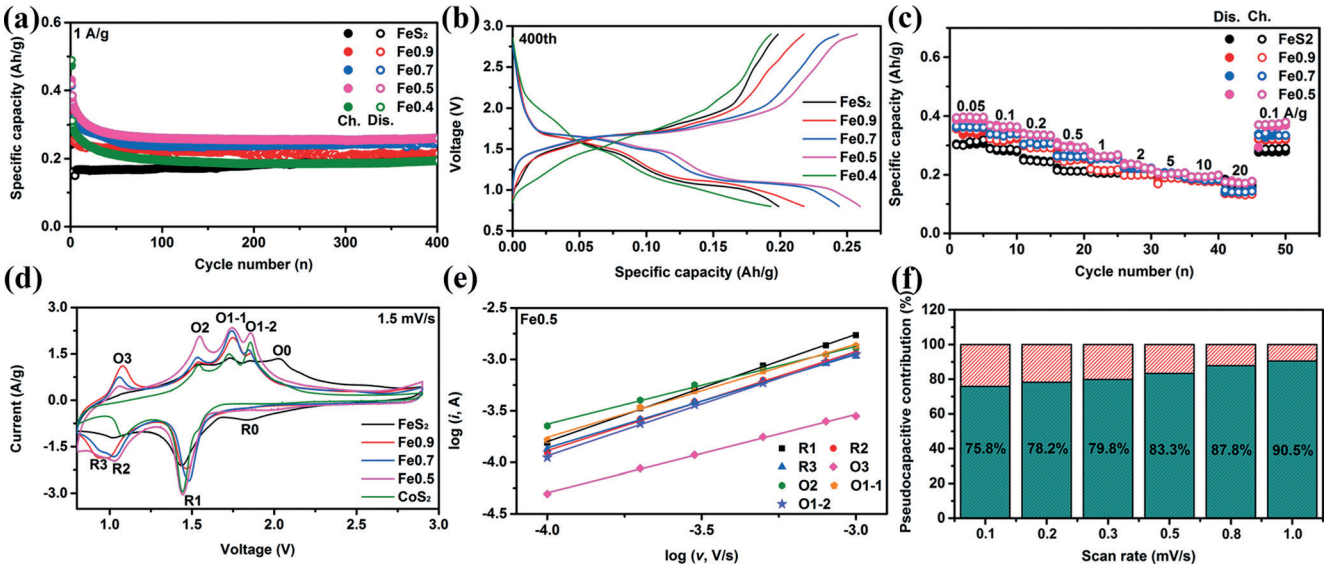

Figure 2. a) Cycling performance and b) charge–discharge curves in the 400th cycle of the as-prepared FeS_2 and four doping samples. c) Rate performance of the as-prepared FeS_2, Fe0.9, Fe0.7, and Fe0.5 samples. d) Typical CV curves of the as-prepared FeS_2, Fe0.9, Fe0.7, Fe0.5, and CoS_2 samples at a scan rate of 1.5 $mV s^{-1}$. e) Log(*i*) vs. log(*v*) plots at each redox peak and f) bar chart showing the percent of pseudocapacitive contribution of the Fe0.5 sample.

that of widely reported $Li_4Ti_5O_{12}$ anodes for LIBs. A moderately high voltage of the anode material can be beneficial to the safety of batteries. Furthermore, Co-doped FeS_2 samples deliver higher capacities than that of $Li_4Ti_5O_{12}$, showing more competitive merit. The charge–discharge voltage curves of the Fe0.4 sample are obviously different from the other curves probably owing to the presence of CoS.

Rate capabilities of the FeS_2, Fe0.9, Fe0.7, and Fe0.5 samples were also characterized (Figure 2c). At low current densities from 0.05 to 1 $A g^{-1}$, the capacities increase as the Co contents increase. At 10 $A g^{-1}$, the capacities of both Fe0.9 and Fe0.7 samples are lower than that of the FeS_2 although they possess higher surface area (Supporting Information, Figure S14) and smaller particle size than those of the FeS_2. Remarkably, the Fe0.5 sample displays the highest capacity among the four samples even at 20 $A g^{-1}$. However, pure CoS_2 only delivers a higher capacity than that of the FeS_2 at a very low rate (0.05 $A g^{-1}$) (Supporting Information, Figures S15, S16). The results indicate that Co-doping increases the capacity but weakens the rate performance. When the ratio of Fe to Co is more than 1:1, the capacity increase does not make up for rate-capability loss. Thus, the Fe0.5 delivers the best performance among all as-prepared samples. Charge–discharge voltage curves of the Fe0.5 sample at different rates are presented in the Supporting Information, Figure S17. Although the differences between charge and discharge voltage plateaus slight increase, the distinct plateaus are observed even at a very high current density of 10 $A g^{-1}$. The Fe0.5 sample shows discharge capacities of 0.261, 0.192, and 0.173 $Ah g^{-1}$ at 1, 10, and 20 $A g^{-1}$, respectively. It can be concluded that the Co-doped FeS_2 samples not only enhance capacities of FeS_2 but also improve the rate performance of CoS_2.

To study the effect of the Co-doping on reaction kinetics, a cyclic voltammetry (CV) test was performed. Figure 2d shows CV curves of the as-prepared FeS_2, Fe0.9, Fe0.7, Fe0.5, and CoS_2 samples. Because the Co-doped FeS_2 and pure FeS_2 and CoS_2 samples display similar redox peaks (R1, R2, O2, O1−1, and O1−2), they should have similar intercalation reactions.[9] To further investigate the rate capability of each reaction, the CV tests at different scan rates were carried out. As shown in the Supporting Information, Figure S18, all peak currents (*i*) increase as the scan rates (*v*) increase. Figure 2e and the Supporting Information, Figure S19 exhibit log(*i*) vs. log(*v*) plots of the five samples at each redox peak, and the slope of the fitted line is denoted by b. A high b-value positively affects rate capability.[4,11] The calculated b-values are listed in the Supporting Information, Table S3. For the Co-doped FeS_2 samples, the b-values of the O2 and O3 peaks are about 0.8, which are higher than that of O2 peak of CoS_2 but lower than that of O2 peak of FeS_2. As a result, the Co-doped FeS_2 samples have higher rate capabilities than CoS_2, but the Fe0.9 and Fe0.7 samples deliver lower capacities at 10 $A g^{-1}$ than that of FeS_2. Figure 2f summarizes contributions of the pseudocapacitive behaviors at various scan rates. The contributions are 75.8%, 78.2%, 79.8%, 83.3%, 87.8%, and 90.5% at the scan rates of 0.1, 0.2, 0.3, 0.5, 0.8, and 1.0 $mV s^{-1}$, respectively. The results reveal that the pseudocapacitive charge-storage amount occupies a relatively high portion of the whole capacity.

Reaction mechanism of the Fe0.5 sample was also investigated. Figure 3a shows in situ XRD analysis of the first cycle. During the discharge process, the characteristic peak of pyrite phase at 32.8° gradually shifts to about 31°, indicating the formation of a monoclinic $NaFe_{0.5}Co_{0.5}S_2$.[9] During the charge process, the peak near 31° gradually changes to about 29°, which is attributed to the transformation from monoclinic $NaFe_{0.5}Co_{0.5}S_2$ to layered $Na_xFe_{0.5}Co_{0.5}S_2$.[9] After about 50 cycles, the active materials totally turn into layered $Na_xFe_{0.5}Co_{0.5}S_2$, but it leads to initial

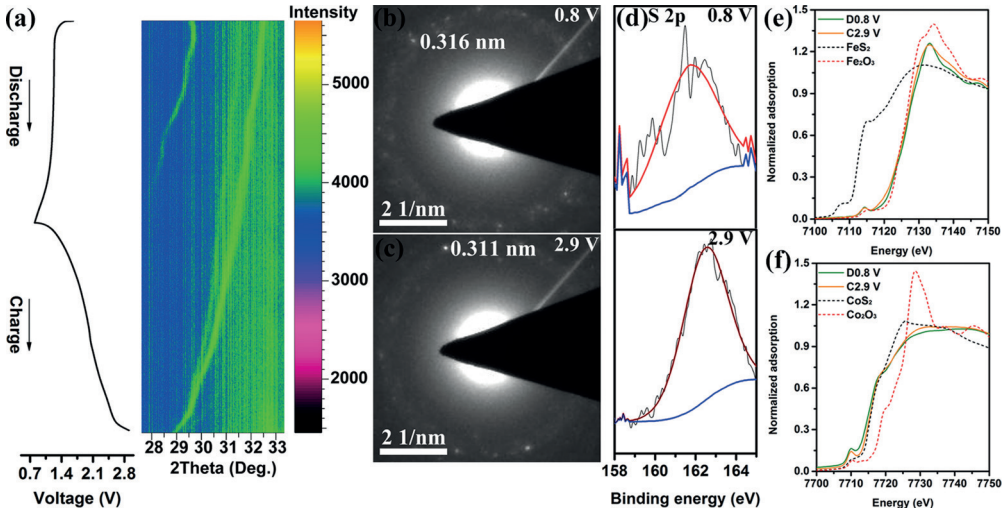

Figure 3. a) In situ XRD analysis of the Fe0.5 electrode during the first cycle and the corresponding image plots of diffraction patterns in a 2θ range of 28–33°. b), c) Ex situ SAED patterns, d) XPS of S 2p peak, and e), f) XANES for Fe (e) and Co (f) of the as-prepared Fe0.5 sample, fully discharged (0.8 V) and charged (2.9 V) after 50 cycles.

capacity declination as shown in Figure 2a. The discharge and charge products in the 50th cycle were also analyzed by ex situ methods. The characteristic d-spaces of 0.316 and 0.311 nm are detected at fully discharged 0.8 V and charged 2.9 V, respectively (Figure 3b,c). It indicates that the layered structure is remained, but interlayer spacing changes during the following cycles.[9] Figure 3d shows ex situ XPS spectra of S 2p peak of the charge–discharge products. The binding energies of S 2p peaks of the discharge and charge products are 161.6 and 162.5 eV, respectively, indicating electrochemical oxidation of S during the charge process. X-ray absorption near-edge spectra (XANES) reveals that cationic valences remain during the charge-discharge process (Figure 3e,f). However, the Fe valence is as similar as that in Fe_2O_3, and the Co valence is close to +2. The results indicate that only intercalation reactions occur when cycling between 0.8 and 2.9 V, which enables good cycle stability.

Figure 4 exhibits composition and cycling performance of the Na/Fe0.5 half-cell and the $Na_3V_2(PO_4)_3$/Fe0.5 full cell. For the half-cell, the discharge capacity is 0.220 Ah g^{-1} after 5000 cycles at 2 A g^{-1}, corresponding to an average capacity retention of about 99.999% per cycle. Furthermore, coulombic efficiencies of the Fe0.5 powder in the 3rd, 1000th, and 5000th cycles are 99.78%, 99.84%, and 99.91%, respectively. The superior Coulombic efficiency is owing to upgradation of discharge terminal voltage and utilization of ether-based electrolyte. Increasing the terminal voltage to 0.8 V avoid the conversion reactions to improve the structural stability, and the ether-based electrolytes have higher chemical stability for polysulfides compared with carbonate-based electrolytes.[9,12] Furthermore, the nanospheres of the Fe0.5 sample are well maintained and homogeneously surrounded by carbon additives after 1000 cycles (Supporting Information, Figure S20), and Fe, Co, and S elements are also dispersed uniformly in bulk of the nanospheres (Supporting Information, Figure S21). The superior electrochemical performance of the Fe0.5 half-cell encouraged us to assemble $Na_3V_2(PO_4)_3$/Fe0.5 full cell. As shown in Figure 4b and the Supporting Information, Figure S22, the full cell with excessive $Na_3V_2(PO_4)_3$ delivers an initial capacity of 0.340 Ah g^{-1} at 0.2 A g^{-1} based on the mass of Fe0.5 with an average output voltage of 1.6 V. The capacity still reaches 0.296 Ah g^{-1} after 100 cycles, corresponding to a capacity retention of 90.2% calculated from the 2nd cycle. The results suggest that the Co-doped FeS_2 can be used for both rechargeable Na and Na-ion batteries. The electrochemical performance of the Fe0.5 is better than those of pure FeS_2 and CoS_2 and comparable to that of $FeSe_2$.[4] Furthermore, S resource has lower toxicity and cost compared with Se resource, which is favorable for large-scale application.

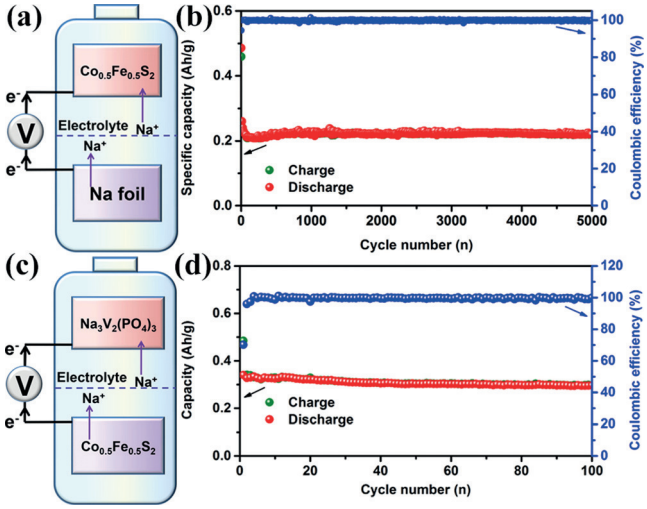

Figure 4. Illustration of the composition and cycling performance of a), b) Na/Fe0.5 half-cell and c), d) $Na_3V_2(PO_4)_3$/Fe0.5 full cell.

In summary, a series of the Co-doped FeS_2 nanospheres have been synthesized by a facile solvothermal method. The optimized $Co_{0.5}Fe_{0.5}S_2$ (Fe0.5) sample delivers a discharge capacity of 0.220 Ah g^{-1} after 5000 cycles at 2 A g^{-1} with an ether-based electrolyte and in a voltage range of 0.8–2.9 V. Even at 20 A g^{-1}, its discharge capacity is still 0.172 Ah g^{-1}. It not only increases the capacity of FeS_2 but also promotes the rate performance of CoS_2. Its redox reactions are mainly controlled by pseudocapacitive behaviors, leading to fast kinetics and durable cyclic life. Furthermore, the $Na_3V_2(PO_4)_3$/Fe0.5 full cell delivers an initial capacity of

0.340 Ah g^{-1} with an average output voltage of 1.6 V. The facile preparation and superior performance of $Co_{0.5}Fe_{0.5}S_2$ nanoshpheres enable them to become a promising anode material for SIBs.

Acknowledgements

This work was supported by the energy efficiency and resources of the Korea Institute of Energy Technology Evaluation and Planning (KETEP) grant funded by the Ministry of Knowledge Economy, Korean government (no: 20152020105420) as well as by the National Research Foundation of Korea (NRF) Grant funded by the Korea government (MSIP) (NRF-2015R1A2A1A15055227) and Chinese 111 Project (B12015).

Keywords: anode materials · cobalt-doped iron disulfides · sodium-ion batteries · solid solutions

How to cite: *Angew. Chem. Int. Ed.* **2016**, *55*, 12822–12826
Angew. Chem. **2016**, *128*, 13014–13018

[1] a) N. Yabuuchi, K. Kubota, M. Dahbi, S. Komaba, *Chem. Rev.* **2014**, *114*, 11636; b) M. S. Islam, C. A. J. Fisher, *Chem. Soc. Rev.* **2014**, *43*, 185; c) Y. S. Yun, K.-Y. Park, B. Lee, S. Y. Cho, Y.-U. Park, S. J. Hong, B. H. Kim, H. Gwon, H. Kim, S. Lee, Y. W. Park, H.-J. Jin, K. Kang, *Adv. Mater.* **2015**, *27*, 6914; d) J. Yang, D.-W. Han, M. R. Jo, K. Song, Y.-I. Kim, S.-L. Chou, H.-K. Liu, Y.-M. Kang, *J. Mater. Chem. A* **2015**, *3*, 1005; e) S. Guo, P. Liu, H. Yu, Y. Zhu, M. Chen, M. Ishida, H. Zhou, *Angew. Chem. Int. Ed.* **2015**, *54*, 5894; *Angew. Chem.* **2015**, *127*, 5992; f) Y. You, X.-L. Wu, Y.-X. Yin, Y.-G. Guo, *Energy Environ. Sci.* **2014**, *7*, 1643.

[2] a) J. Liu, P. Kopold, C. Wu, P. A. van Aken, J. Maier, Y. Yu, *Energy Environ. Sci.* **2015**, *8*, 3531; b) Y. Liu, N. Zhang, L. Jiao, J. Chen, *Adv. Mater.* **2015**, *27*, 6702; c) W. Li, S.-L. Chou, J.-Z. Wang, J. H. Kim, H.-K. Liu, S.-X. Dou, *Adv. Mater.* **2014**, *26*, 4037; d) Y. Zhang, X. Rui, Y. Tang, Y. Liu, J. Wei, S. Chen, W. R. Leow, W. Li, Y. Liu, J. Deng, B. Ma, Q. Yan, X. Chen, *Adv. Energy Mater.* **2016**, *6*, 1502409.

[3] C. Zhu, X. Mu, P. A. van Aken, Y. Yu, J. Maier, *Angew. Chem. Int. Ed.* **2014**, *53*, 2152; *Angew. Chem.* **2014**, *126*, 2184.

[4] K. Zhang, Z. Hu, X. Liu, Z. Tao, J. Chen, *Adv. Mater.* **2015**, *27*, 3305.

[5] Z. Hu, L. Wang, K. Zhang, J. Wang, F. Cheng, Z. Tao, J. Chen, *Angew. Chem. Int. Ed.* **2014**, *53*, 12794; *Angew. Chem.* **2014**, *126*, 13008.

[6] Z. Shadike, M.-H. Cao, F. Ding, L. Sang, Z.-W. Fu, *Chem. Commun.* **2015**, *51*, 10486.

[7] a) Y. Zhang, P. Zhu, L. Huang, J. Xie, S. Zhang, G. Cao, X. Zhao, *Adv. Funct. Mater.* **2015**, *25*, 481; b) S. S. Zhang, *J. Mater. Chem. A* **2015**, *3*, 7689; c) H. Yoo, A. P. Tiwari, J. Lee, D. Kim, J. H. Park, H. Lee, *Nanoscale* **2015**, *7*, 3404.

[8] W. Luo, F. Shen, C. Bommier, H. Zhu, X. Ji, L. Hu, *Acc. Chem. Res.* **2016**, *49*, 231.

[9] Z. Hu, Z. Q. Zhu, F. Y. Cheng, K. Zhang, J. B. Wang, C. C. Chen, J. Chen, *Energy Environ. Sci.* **2015**, *8*, 1309.

[10] J. M. Clamagirand, J. R. Ares, E. Flores, P. Diaz-Chao, F. Leardini, I. J. Ferrer, C. Sánchez, *Thin Solid Films* **2016**, *600*, 19.

[11] T. Brezesinski, J. Wang, S. H. Tolbert, B. Dunn, *Nat. Mater.* **2010**, *9*, 146.

[12] Z. Hu, Q. Liu, W. Sun, W. Li, Z. Tao, S.-L. Chou, J. Chen, S.-X. Dou, *Inorg. Chem. Front.* **2016**, *3*, 532.

Received: August 2, 2016
Published online: September 14, 2016

